Functional connectivity, tissue microstructure and T2 at 11.1 Tesla distinguishes neuroadaptive differences in two traumatic brain injury models in rats: A Translational Outcomes Project in NeuroTrauma (TOP-NT) UG3 phase study

**Rohan S. Kommireddy[2], **Shray Mehra[2], Marjory Pompilus[2], Rawad Daniel Arja[1], Tian Zhu[1], Zhihui Yang[1,3], Yueqiang Fu[1], Jiepei Zhu[1], Firas Kobeissy[1-4], *Kevin K.W. Wang[1-4], *Marcelo Febo[2]

(*co-senior authors; **equal contributions)

Author affiliations:

1 Program for Neurotrauma, Neuroproteomics & Biomarkers Research, Department of Emergency Medicine, University of Florida, 1149 South Newell Drive, Gainesville, FL 32611

2 Department of Psychiatry, McKnight Brain Institute, University of Florida, 1149 South Newell Drive, Gainesville, FL 32611

3 Brain Rehabilitation Research Center, Malcom Randall VA Medical Center, 1601 SW Archer Rd. Gainesville FL 32608-1197

4 Department of Neurobiology, Center for Neurotrauma, Multiomics & Biomarkers (CNMB), Neuroscience Institute, Morehouse School of Medicine, 720 Westview Dr SW, Atlanta, GA 30310-1458, USA

Co-Corresponding authors: Kevin K.W. Wang, PhD and Marcelo Febo, PhD

Contact information: Dr. Marcelo Febo, Department of Psychiatry, P.O. Box 100256, Gainesville, Florida 32611; Office: (352) 294 4911; Email: febo@ufl.edu

Running title: Neuroimaging biomarkers for brain injury

Keywords: Traumatic brain injury; controlled cortical impact; lateral fluid percussive injury, neuroimaging, tissue microstructure, functional connectivity, relaxometry

Abstract

The damage caused by contusive traumatic brain injuries (TBIs) is thought to involve breakdown in neuronal communication through focal and diffuse axonal injury along with alterations to the neuronal chemical environment, which adversely affects neuronal networks beyond the injury epicenter(s). In the present study, functional connectivity along with brain tissue microstructure coupled with T2 relaxometry were assessed in two experimental TBI models in rat, controlled cortical impact (CCI) and lateral fluid percussive injury (LFPI). Rats were scanned on an 11.1 Tesla scanner on days 2 and 30 following either CCI or LFPI. Naive controls were scanned once and used as a baseline comparison for both TBI groups. Scanning included functional magnetic resonance imaging (fMRI), diffusion weighted images (DWI), and multi-echo T2 images. fMRI scans were analyzed for functional connectivity across laterally and medially located region of interests (ROIs) across the cortical mantle, hippocampus, and dorsal striatum. DWI scans were processed to generate maps of fractional anisotropy, mean, axial, and radial diffusivities (FA, MD, AD, RD). The analyses focused on cortical and white matter (WM) regions at or near the TBI epicenter. Our results indicate that rats exposed to CCI and LFPI had significantly increased contralateral intra-cortical connectivity at 2 days post-injury. This was observed across similar areas of the cortex in both groups. The increased contralateral connectivity was still observed by day 30 in CCI, but not LFPI rats. Although both CCI and LFPI had changes in WM and cortical FA and diffusivities, WM changes were most predominant in CCI and cortical changes in LFPI. Our results provide support for the use of multimodal MR imaging for different types of contusive and skull-penetrating injury.

Introduction

Traumatic brain injury (TBI) afflicts millions worldwide, with mortality rates over 30%[1]. Although mild-to-moderate repetitive closed head injuries are the most prevalent among the different types of TBI, focal contusions and skull penetrating injuries caused by forceful blows, jolts, bumps to the head, neck, or spinal cord result in devastating outcomes. The long-term, lifelong sensorimotor, emotional, and cognitive impairments, and permanent disruptions to brain function and structure, with severe TBI exert a heavy emotional and financial toll on patients and caregivers. The heterogeneity of damage to the brain with severe TBI makes it difficult to clinically manage. The pathophysiology of contusive injuries involves mechanistically heterogeneous and complex cellular and molecular mechanisms extending beyond the primary site of injury. These so-called secondary injuries can involve aberrant inflammatory neuroimmune activity, diffuse axonal injury (DAI) and other forms of white matter (WM) damage, blood-brain barrier (BBB) disruption, microvasculature bleeds, intracranial hematomas, cerebral and subdural hemorrhage and edema, epileptiform activity, and other adaptive central nervous system (CNS) pathologies[2]. Clinical TBI treatment and management relies on the earliest possible interventions to curb the progression of these secondary injuries[3]. Despite the reported neuroprotective effects of experimental drugs in animal models of TBI, none have proven effective in clinical trials[4]. This failure can be attributed in part to a lack of data on *in vivo*, minimally invasive translational CNS markers to bridge preclinical mechanisms to clinical TBI[4].

Functional neuroimaging offers translational data that may help close in on clinically relevant mechanisms of disease progression and behavioral recovery in TBI, especially when analyzed together with other quantitative magnetic resonance imaging modalities. For instance, neuroimaging of a diverse cohort of mild-to-severe TBI identified stronger deactivations of the default mode network (DMN) regions during cognitive task performance and a negative relationship between posterior cingulate functional connectivity and mean diffusivity (MD) in splenium[5]. Similar brain areas were observed to have reduced connectivity following mild TBI[6], although hyper-connectivity within DMN regions has also been reported[7] and is associated with metacognitive recovery following moderate to severe TBI[8]. Both increases and decreases in functional connectivity between limbic, sensorimotor, and association cortical areas have been observed over extended periods following moderate to severe TBI[9], and in mild concussive injuries[10]. Individuals sustaining sports-related mild concussions have decreased long-distance and increased local functional connectivity[11]. Thus, despite heterogeneity in the extent of direct or secondary damage caused by TBI, consistency can be said to emerge from results showing temporally evolving functional connectivity reductions and increases across cortical subregions.

Whether or not such changes are specifically restricted to cognitive, motor, sensory, or association cortices over time remains unclear. Animal studies recapitulating mild concussive injuries caused by sports injuries or automobile accidents are necessary to model prevalent forms of TBI in humans[12,13]. Like clinical TBI, however, these produce diffuse and heterogenous pathology that, while invaluable to determining construct validity of preclinical TBI models, have so far shown limited ability to reveal fundamental mechanisms involved in cortical reorganization observed with contusions and penetrating cortical injuries. Preclinical studies using controlled cortical impact (CCI) and lateral fluid percussive impact (LFPI) models consistently demonstrate functional reorganization of the cortex near and distant from the TBI epicenter[14]. The large-scale functional network reorganization continues over 30 to 60 days[15,16] and may involve excitatory-inhibitory rebalancing following TBI[17]. These cortical changes are likely accompanied by changes in WM microstructure[18] and chemical changes measurable by tissue T2 relaxometry[19]. The objective of the present study was to assess functional connectivity together with brain tissue microstructure and T2 relaxometry in CCI and LFPI models to evaluate salient similarities and differences between these models.

Materials and Methods

Subjects

Female and male Sprague-Dawley rats (220-300g; N=89) were obtained from Charles River Laboratories (Raleigh, NC, USA.). Rats were housed in sex-matched pairs in a temperature and humidity-controlled vivarium with a 12 h light cycle (lights on at 0700 h) and food and water provided ad libitum. Rats were randomly assigned to one of three experimental conditions: controls (n=26; 18 male and 8 female rats), CCI (n=30; 17 male and 13 female rats), and LFPI (n=13; 8 male and 5 female rats). Controls received anatomical and functional MRI scanning in a single session. CCI and LFPI groups received anatomical and fMRI scanning at 2 days post-injury and a smaller subset were scanned on 30-days post-injury. The latter subset included 12 CCI (4 males, 8 females) and 8 male LFPI rats. The number of rats that received diffusion weighted imaging (DWI) and T2 relaxometry were lower than for fMRI due to the removal of scans. The number of rats receiving DWI and T2 scans are provided in corresponding figure legends. All procedures received prior approval from the Institutional Animal Care and Use Committee of the University of Florida and followed all applicable NIH guidelines.

Controlled Cortical Impact (CCI)

The CCI procedure was carried out using a Leica Impact One device (Leica Microsystems Inc). Anesthetic levels were induced with 4% isoflurane gas mixed with 100% oxygen and maintained under 2% isoflurane for the rest of the procedure. The body temperature was regulated to 37°C using a thermal pad while rats were prepared for surgery on a stereotaxic frame. A parasagittal craniectomy (center at anteroposterior [AP], -4.0 mm; L, +2.8 mm from lambda) 5 mm in diameter was performed to expose the brain and allow impactor tip access to the cortical surface. The impactor had a 4-mm flat-face tip. CCI at a depth of 1.5 mm at 4 m/s and a dwell time of 240ms was carried out. All injuries occurred in the right hemisphere. The surgical area was sutured, and recovery was monitored by tail pinch and righting reflexes. Control rats were naïve and received no sham surgical procedures.

Lateral Fluid Percussion Injury (LFPI)

To model diffuse and focal, open-head TBI, and as part of the translational outcomes project in neurotrauma (TOP-NT), we used the rat LFPI model. LFPI is a well-characterized model of TBI that captures clinically relevant deficits and pathologies[20-22]. LFPI also applies a localized, mechanical insult through a parasagittal craniectomy; however, LFPI is administered via a pressurized fluid pulse (2.0 ±0.2atm). This injury results in a moderated diffuse and focal injury on the right sensorimotor cortex and expansive and progressing white matter injury[2]. Even in cases where limited histopathology is observed, LFPI subjects exhibit manifold neurobehavioral deficits[21,23]. This is consistent with the literature where the majority of TBI cases do not present overt pathology on imaging assessments, yet patients experience lasting and debilitating symptoms.

Magnetic Resonance Imaging (MRI)

Images were collected in an 11.1 Tesla MRI scanner (Magnex Scientific Ltd., Oxford, UK) with a Resonance Research Inc. gradient set (RRI BFG-240/120-S6, maximum gradient strength of 1000 mT/m at 325 Amps and a 200 µs risetime; RRI, Billerica, MA) and controlled by a Bruker Paravision 6.01 console (Bruker BioSpin, Billerica, MA). A custom-made 2.5 cm x 3.5 cm quadrature radiofrequency (RF) surface transmit/receive coil tuned to 470.7MHz (^{1}H resonance) was used for B1 excitation and signal detection (RF engineering lab, Advanced Magnetic Resonance Imaging and Spectroscopy Facility, Gainesville, FL). Rats were scanned under a continuous flow of 1.5 % isoflurane (delivered at 0.1L/min mixed with medical-grade air containing 70% nitrogen and 30% oxygen). Respiratory rates were monitored continuously, and

body temperature was maintained at 36-37°C using a warm water recirculation system (SA Instruments, Inc., New York).

For each rat, a high-resolution T2 weighted anatomical scan followed by a functional magnetic resonance imaging (fMRI) scan, a diffusion weighted imaging (DWI) scan, and a multi-echo time image series for T2 mapping were acquired. T2-weighted Turbo Rapid Acquisition with Refocused Echoes (TurboRARE) scans were acquired with the following parameters: effective echo time (TE) = 37 ms, repetition time (TR) = 5 seconds, RARE factor = 16, number of averages = 14, field of view (FOV) of 24 mm x 18 mm and 0.9 mm thick slice, and a data matrix of 256 x 192 and 25 interleaved ascending coronal (axial) slices covering the entire brain from the rostral-most extent of the anterior frontal cortical surface, caudally towards the upper brainstem and cerebellum. Functional images were collected using a single-shot spin-echo echo planar imaging (EPI) sequence with the following parameters: TE = 15 ms, TR = 2 seconds, 300 repetitions, FOV = 24 x 18 mm and 0.9 mm thick slice, and a data matrix of 64 x 48 with 25 interleaved ascending coronal slices in the same space as the T2 anatomical. Respiratory rates, isoflurane concentration, body temperature, lighting, and room conditions were kept constant across subjects. Diffusion images used a 4-shot spin echo EPI readout with TE=18ms, TR=4 seconds, 4 averages, FOV = 24 x 18 mm and 0.9 mm slices and a data matrix of 128 x 96 x 25, 30 directions with a b value = 900 s^2/mm and 4 b = 0 scan, pulse duration = 3 ms, and gradient separation = 8 ms. Multi-slice multi-echo scans were collected with TE=6-60 ms in 6 ms steps per image volume, TR=2 seconds, 2 averages, FOV = 24 x 18 mm with 0.9 mm slices and a data matrix of 128 x 128 x 25.

Functional MRI Processing

Image processing was conducted using software tools available in Analysis of Functional NeuroImages (AFNI)[24], FSL[25], and Advanced Normalization Tools (ANTs)[26] and manual mask drawing and editing functions in ITKSNAP[27]. Masks outlining the brains of rats on fMRI, DWI, and T2 anatomical scans were generated using *3dAutomask* in AFNI. These were used for brain extraction in various steps in the image processing workflows. The processing of fMRI scans included the following steps: (1) timeseries spike identification and removal using *3dDespike* in AFNI, (2) motion correction using *3dvolreg* in AFNI, (3) removal of slow signal drifts (<0.009Hz) using *3dTproject* in AFNI, (4) identification and suppression of nuisance signals using *fsl_regfilt* in FSL, (5) low-pass filtering (>0.12Hz) and spatial smoothing (0.6mm FWHM), and (6) linear affine followed by non-linear registrations of cropped fMRI scans to cropped anatomical scans using *flirt* in FSL and the *antsRegistrationSyNQuick* script for ANTs.

Anatomical co-registration matrices were applied to fMRI scans to align these to a multi-T2 scan template upon which ROIs were created. The template was generated by first using rigid-body and affine co-registration steps and then a final nonlinear symmetric normalization step in ANTs. A total of 52 bilateral ROIs were manually created in ITKSNAP. These spanned in an axial slice arrangement the medial and lateral regions of the rostral-to-caudal cortical mantle, hippocampus and dorsal striatum (**Figure 1A-C**). These ROIs were used for signal extraction for seed based functional connectivity.

This generated 52 individual ROI text files per subject that contained L2-normalized resting state signals as a vector of 300 data points. The timeseries files were used in cross-correlations and in calculations of Pearson r coefficients for every pairwise combinations of ROIs (using *corrcoef* function in MATLAB). The resulting number of pairwise correlations was 1,274 per subject (after removing 52 self-correlations). Correlation coefficients were Fisher's transform to ensure normality prior to statistical analyses. The 52 ROIs and template were visualized in 3D using BrainNet viewer [28]. Weighted undirected matrices derived from the Pearson correlations were analyzed using Brain Connectivity Toolbox [29] in MATLAB (Mathworks, Natick, MA). Global graph metrics were calculated for edge density thresholds ranging from 2-40%. Global network measures for this density range were converted to area under the curve (AUC) values prior to statistical analyses. Node-specific (ROI) network measures were calculated at a 12% threshold. The functional network analysis was focused on measuring node strength (sum of edge weights/node) in subregions of the cortex, hippocampus and striatum.

Diffusion Weighted Image (DWI) Processing

ITKSNAP was used to segment contralateral and ipsilateral cortical and white matter ROIs. Diffusion MRI scans were processed using tools available on FSL [30]. DWI scans were first screened for volumes with low signal-to-noise or artefacts. Eddy correction was used for adjusting slight movements during image acquisition and gradient files rotated according to the motion correction vectors. After eddy correction, tensor element reconstruction and estimates of eigenvectors and eigenvalues were performed using weighted least squares regression on *dtifit* in FSL. This last step generated independent images of FA, mean, axial and radial diffusivities (MD, AD, and RD, respectively).

T2 Mapping

T2 parametric maps were created using the MRI processor plugin for ImageJ[31,32]. The simplex minimization method was used for the non-linear fit of multi-TR images to the equation $S_{TE} = S_0 * e^{-TE/T2}$). ITKSNAP was used to segment contralateral and ipsilateral cortical and white matter ROIs, similar to DWI scans. From T2 maps, the mean T2 is calculated per ROI and exported for statistical analysis.

Statistical Analysis

Statistical analyses and data plotting were carried out using GraphPad Prism 9. Functional connectivity data were analyzed using linear mixed effects (LME) analysis of variance (ANOVA) with repeated measures. A two-stage step-up false discovery rate method was used for multiple comparisons correction. DWI scalars and T2 data were analyzed using a two-way ANOVA with Tukey's honest significant difference post hoc test.

Results

Differential Patterns of Recovery of Functional Connectivity in CCI and LFPI

Functional connectivity within and between contralateral and ipsilateral nodes was evaluated in the medial and lateral areas of the cortex, as well as the hippocampus and striatum, on days 2 and 30 post-injury (ROIs are shown in **Figure 1**). **Figure 2A-E** highlights the average node strength in 3D connectome maps of control, CCI, and LFPI, on days 2 ad 30 post-injury. The 3D maps illustrate a higher node strength in the contralateral cortex of CCI and LFPI animals on day 2. The greater node strength is observed on both days 2 and 30 for CCI rats, but only day 2 in LFPI rats. The 3D maps also show an increase in intra-hemispheric functional connectivity (an increase in the number of node-connecting edges) within the contralateral cortex.

A closer evaluation of the CCI and LFPI groups in the heat map in **Figure 2F** revealed that in the contralateral medial cortex, in the rostral and most caudal areas, are significantly greater in node strength on days 2 and 30 compared to controls (group x ROI: $F_{204,4284}=2.5$, $p<0.0001$; **Figure 2F** highlights FDR corrected pairwise t-test comparisons for all groups). The lateral subregion of the contralateral cortex of CCI rats had significantly greater node strength on both days 2 and 30 post-injury compared to controls but in a limited single slice. In the ipsilateral cortex, the medial subregion had significantly lower node strength on both days 2 and 30 compared to controls. This was limited to the more caudal areas of the cortex, within the range of the injury epicenter. The CCI-induced reductions in node strength extended to the lateral areas of the ipsilateral cortex.

In LFPI rats, the increased node strength in the contralateral cortex was observed 2 days, but not 30 days, post-injury (**Figure 2F** shows FDR corrected pairwise t-test comparisons). The ipsilateral cortex had significant reductions in node strength, most prominently in the medial cortical areas, although lateral areas of the posterior region of the cortex also had low node strength in LFPI rats relative to controls. The observed reductions in ipsilateral cortical node strength in LFPI rats were observed on day 2 post-injury and recovered to control levels in both lateral and medial areas of the cortex by day 30.

Figure 3 summarizes the functional changes observed in cortical regions of CCI and LFPI rats. Both CCI and LFPI rats had significant contralateral increases and ipsilateral decreases in node strength, which we use here as a surrogate marker of functional connectivity. The observed functional changes were observed in primary sensory areas (e.g., somatosensory, auditory, visual) and primary motor cortex on day 2 post-injury in both models (**Figure 3A** and **3C**). By 30 days after injury, significant decreases in ipsilateral node strength are still observed near the injury epicenter in CCI rats. No differences were observed in LFPI rats.

Distinct White Matter and Cortical Diffusion Changes and Differential Recovery in CCI and LFPI Models

Figure 4 shows representative DWI and T2 scans collected in a control, CCI and LFPI rats at 11.1 Tesla, illustrating the slice range where the epicenter was generally located on each of these maps. We analyzed FA, MD, AD, and RD in ipsi and contralateral WM and cortex. The ROIs included the cortical TBI epicenter and its corresponding section of corpus callosum WM tissue. CCI rats had reduced FA in ipsilateral WM (group: $F_{2,78}$=38.5, p<0.0001; day: $F_{1,78}$=34.2, p<0.0001; post hoc comparisons indicated in **Figure 5**) and contralateral WM (group: $F_{2,78}$=11.4, p=0.001; day: $F_{1,78}$=23.2, p<0.0001) on day 2 post-injury (**Figure 5A**). FA returned to control levels in these brain tissues by day 30 post-CCI. Compared to the control groups, LFPI rats had reduced FA in ipsilateral WM on day 2 post-TBI (**Figure 5A**). No differences in FA between controls and LFPI rats were observed in contralateral WM and contralateral cortex (**Figure 5A**). MD in ipsilateral WM was greater in CCI compared to controls on day 2, but not day 30 (group: $F_{2,78}$=10.2, p=0.0001; day: $F_{1,78}$=19.2, p<0.0001). No differences in MD between control and CCI rats were observed in contralateral WM, and ipsilateral and contralateral cortex (**Figure 5B**). MD increased compared to controls in ipsilateral cortex on day 30 post-TBI (**Figure 5B**). No differences in MD between control and LFPI rats were observed in WM ROIs (**Figure 5B**). AD in ipsilateral and contralateral WM was reduced in CCI rats on day 30 relative to CCI on day 2,

and increased on ipsilateral cortex on day 30 relative to day 2 for the same group (day [ipsilateral WM]: $F_{1,77}$=14.6, p=0.0003; day [contralateral WM]: $F_{1,76}$=10.3, p=0.002; day [ipsilateral cortex]: $F_{1,78}$=30.5, p<0.0001). No differences in AD between controls and CCI rats were observed in the cortex (**Figure 5C**). AD was lower in ipsilateral and contralateral WM and greater in the ipsilateral cortex on day 30 in LFPI rats compared to LFPI on day 2. No differences in AD between control and LFPI rats were observed in contralateral cortex (**Figure 5C**). RD in ipsilateral and contralateral WM was reduced in CCI rats on day 30 relative to CCI on day 2, and increased on ipsilateral cortex on day 30 relative to day 2 for the same group (day [ipsilateral WM]: $F_{1,77}$=10.2, p=0.002; group [ipsilateral WM]: $F_{2,77}$=7.0, p=0.002; day [contralateral WM]: $F_{1,77}$=4.2, p=0.04; group [ipsilateral cortex]: $F_{2,77}$=5.9, p=0.004; day [contralateral WM]: $F_{1,78}$=23.2, p<0.0001; group [ipsilateral cortex]: $F_{2,77}$=5.9, p=0.004; day [contralateral cortex]: $F_{2,76}$=5.3, p=0.007). Compared to the control group, RD was reduced in CCI day 30 in the ipsilateral cortex (**Figure 5D**). RD was lower in ipsilateral and contralateral WM and contralateral cortex., and greater in the ipsilateral cortex on day 30 in LFPI rats compared to LFPI on day 2 and the group. No differences in RD between control and LFPI rats were observed in contralateral cortex (**Figure 5D**).

Distinct White Matter and Cortical T2 Relaxation Changes and Recovery in CCI and LFPI Models

We analyzed tissue T2 values (in ms) in ipsilateral and contralateral WM and cortex. Compared to controls, T2 was increased in ipsilateral WM (group: $F_{2,56}$=8.6, p = 0.0006; day: $F_{1,56}$=10.7, p = 0.002; post hoc test results indicated in **Figure 6**), contralateral WM (group: $F_{2,56}$=5.1, p = 0.009; day: $F_{1,56}$=4.2, p = 0.04) and in ipsilateral cortex (group: $F_{2,56}$=4.6, p = 0.01) of CCI rats on day 2 post-TBI. T2 values in these brain areas of CCI rats recovered to control levels on day 30. No differences in T2 between control and CCI rats were observed in the contralateral cortex. Compared to controls, T2 values in ipsilateral WM and contralateral WM were greater in LFPI rats on day 2. T2 in these WM areas of LFPI rats recovered to control values by day 30 post-injury. No differences in T2 between control and LFPI rats were observed in ipsilateral and contralateral cortex.

Discussion

The results show important similarities and differences in cortical functional connectivity between CCI and LFPI groups. Both CCI and LFPI rats had significantly increased contralateral intra-cortical connectivity at 2 days post-injury. This was observed across a similar section of the

cortex in the medial and lateral areas of the cortical mantle. The increased contralateral connectivity was still observed by day 30 in CCI, but not LFPI rats. While we did not include additional measures, based on the existing hypothesis suggesting excitatory-inhibitory rebalancing[14], it is possible that such changes in neuroadaptive processing continue in CCI animals, and it is established in LFPI. As expected, and reported previously in CCI rats by Yang et al[15], we observed functional connectivity reductions in the ipsilateral cortex in both groups. However, once again, we observed that reduced functional connectivity at or near the injury site is no longer observed by day 30 in LFPI rats, but it endures in both medial and lateral cortical areas in CCI rats. The cortical areas affected in CCI and LFPI included cross-modal sensory regions and motor cortex. These results suggest that comparisons between CCI and LFPI might provide insight into potential cortical neuronal adaptive mechanisms that may be important to functional recovery. To determine links between cortical functional changes and tissue microstructure, we assessed DTI-processed DWI scans. Although both CCI and LFPI had changes in WM and cortical FA and diffusivities, WM changes were most predominant in CCI and cortical changes in LFPI. This result could be related to the above proposition that LFPI rats had an appreciable recovery by day 30, possibly in association with a rebalancing of neuronal activity across the sensorimotor cortex. The hypothesized changes could involve axonal modifications to compensate for functional losses, as observed in recovery processes in other injury models[33-35], and this, in turn, can impact axial and radial diffusivities. In the contralateral cortex of LFPI rats we observed an increased axial diffusivity and reduced radial diffusivity, which is suggestive of an increase in the directionality of fibers. Finally, T2 values in ipsilateral- and contralateral WM and cortex were similar in CCI and LFPI rats. The increased T2 values on day 2 recovered to control levels by day 30. The similarities between ipsilateral and contralateral regions in both models are interesting. While increased edematous tissue at 2 days could increase T2 at the epicenter, it may be plausible that this also infiltrates the contralateral region[19]. Histological assessments, particularly 3D whole-brain methods may be able to provide mechanistic insight.

Changes in cortical excitability have been reported in rats exposed to either CCI or LFPI, and this has been largely attributed to the development of post-trauma epilepsy (PTE). Both spontaneous and evoked discharges were reported in layer 5 pyramidal neurons, which additionally showed increased burst durations during the first 2 weeks post-CCI[36]. Reduced frequency of spontaneous inhibitory postsynaptic currents (sIPSC), possibly involving reduced gamma amino butyric acid (GABA) release locally, has also been reported[17]. Increases in functional connectivity in the contralateral cortex in both LFPI and CCI models may thus

correspond to widespread changes in excitability involved in PTE. However, there is evidence suggesting the mechanisms may be more nuanced. For example, decreased functional connectivity in the cortex has been reported in rats also experiencing shorter latencies to seize and increased interictal epileptic discharges (IEDs)[37]. Besides the role altered neurovascular coupling is likely to play in both reductions and increases in functional connectivity following TBI, increased spontaneous firing across multiple neocortical areas should substantially elevate neuronal oxygen demand and increase blood oxygenation level-dependent (BOLD) signal fluctuations. Synchronous BOLD activity is expected to increase non-specifically, and in a widespread manner, in this scenario. Harris and co-workers reported evidence that this hyperexcitability can be reduced by local inhibitory effects of infused potassium in the contralateral cortex [38]. They posit that this hyperexcitability may be due to the loss of ipsilateral cross-callosal excitatory fibers that modulate contralateral inhibitory neurons (contributing to overexcitability by releasing inhibitory modulation)[38]. The relationship between changes in neuronal excitability and synchronous BOLD activity is not a linear one. Inhibition of mitochondrial function reduces both spontaneous neuronal discharges and functional connectivity, while elevated mitochondrial activity increases neuronal discharges but still reduces cortical functional connectivity[39]. Our neuroimaging results, and behavioral results reported by others[40], suggest significant functional recovery over 30 days or more, further reinforcing the notion of compensatory neuroadaptations that may involve reorganization of neuronal activity in the cortex of CCI and LFPI rats. PTE-related changes may be accompanied by changes in functional network topology (perhaps contributing to behavioral recovery)[14,15].

The observed functional connectivity changes can also be attributed to altered neurovascular coupling[41]. Increased BBB permeability, astrocytosis, synaptic loss, and damage to microvessels are indicative of a failing neurovascular unit. A result of TBI-induced neurovascular changes is an alteration in cerebral blood flow (CBF). CBF changes have been reported early – within hours - post-injury and at 1 year[42,43]. The CBF changes with TBI involve changes in hypercapnia reactivity, suggesting changes in smooth muscle vasodilatory responsiveness in contralateral and ipsilateral cortices[44-46]. At 3 h, CBF is reduced globally by CCI by as much as 85% in ipsilateral and 49% in contralateral cortex[47]. Mild LFPI produced slight but significant differences in CBF and cerebral blood volume (CBV) between ipsilateral and contralateral cortex at 12 hours post-injury[42]. On the other hand, at 1-year post-injury, CCI reduced CBF at the TBI epicenter, including part of the hippocampus. However, no differences in CBF were observed in contralateral cortex[43]. This latter result suggests a certain degree of neurovascular recovery takes place in off-epicenter sites of the cortex, particularly in the

contralateral cortex. Thus, functional connectivity changes in these off-TBI regions are likely to involve neuronal activity changes and are not entirely due to altered CBF mechanisms.

Our DTI analysis focused on corpus callosum segments circumventing the TBI epicenter and in the contralateral cortex. We also assessed the cortical epicenter area and corresponding contralateral cortex to evaluate tissue microstructural differences at 2 and 30 days. Based on the literature, the reported changes in DTI scalars, either using a similar ROI analysis or whole-brain statistics, appear highly heterogeneous across laboratories. Using the CCI model, Harris and colleagues reported ipsilateral WM FA reductions and corresponding diffusivity changes at 1 week, which persisted through 4 weeks[18]. The results were supported by histological data showing demyelinated fibers[18]. This contrasts with our present results using an a priori ROI approach and the difference is likely due to their more comprehensive WM tract-based statistics approach. Changes in WM can surpass localized changes near the epicenter, particularly at later stages post-injury[18]. Conversely, CCI-induced reductions in FA in callosal WM recovered to control levels by day 28 post-TBI, but MD persisted to this time point[48]. Others have reported reductions in FA that were observed 6 months after CCI exposure in rats[16]. This was accompanied by decreases in AD and increased RD[16]. The observed reductions in FA (and increased MD) are associated with significant increases in activated microglia marker translocator protein 18kDa (TSPO), *in vivo*[49]. Yet another study using CCI model reports reductions in FA and increases in MD at 2 days but not at 3 h or 7 days or later[50]. While these results call for improvements in the standardization of DWI methods to facilitate cross-laboratory comparisons, they also suggest the possibility that the neuroadaptations in WM carry large inter-subject (and perhaps, intra-subject) variability. The cellular and molecular changes guiding WM restructuring and axonal remodeling following TBI are likely to involve a certain degree of spatial and temporal ‘randomness’, even with focal contusion models, that could make it difficult to consistently measure the same results using DWI/DTI across and within research laboratories. Our results also indicate increases in T2 in ipsilateral and contralateral cortex and WM at day 2 that is no longer observed on day 30. CCI-induced increased T2 correlates with tissue edema and this in turn has been linked with increases in aquaporin-4 in cortex[19]. The temporal evolution of changes in T2 varies across laboratories as well. Recovery of T2 to control levels in the perilesional or contralateral cortex has been reported at 7 days[50], 14 days[45], and 30 days (present study), or not recovery by a 42nd day of imaging post-CCI[19]. Manninen et al report increases in T2 at day 2 post-FPI and reductions in T2 compared to naïve controls by day 7, with the same effect observed again on day 21[51]. The latter could be a sign of permanent tissue damage at later time points.

Conclusions

In conclusion, our results provide additional support for the use of multimodal MR imaging to determine the *in vivo*, progressive changes in function and tissue microstructure following contusive and skull penetrating injury. Both fMRI and DWI are potentially capable of distinguishing pathological changes between LFPI and CCI models. However, comparisons with the literature strongly suggest the need for methodological standardization, data harmonization, and statistical approaches to facilitate cross-laboratory comparisons, feature extraction, and/or classifications with enough information to evaluate potentially important preclinical findings relevant to clinical TBI[52,53].

Acknowledgements

This study was funded by the National Institute on Neurological Disorders and Stroke Translational Outcomes Project in Neurotrauma (TOP-NT) Award (UG3NS106938 to K.K.W.) and generous funding from the Vivian L. Smith Foundation. We acknowledge the constructive discussions with Dr. Patrick Bellgowan, Dr. Carol Taylor-Burds, and Dr. Hibah Awwad of NIH NINDS and other TOP-NT consortium investigators. The contents of this manuscript are solely the responsibility of the authors and do not necessarily represent the official views of the funding agencies. This work was performed in the McKnight Brain Institute at the National High Magnetic Field Laboratory's AMRIS Facility, which is supported by National Science Foundation Cooperative Agreement No. DMR-1644779 and the State of Florida.

Author Confirmation/Contribution Statement

Rohan S. Kommireddy: investigation, writing (original draft; equal), formal analysis. **Shray Mehra:** investigation, writing (original draft; equal), formal analysis. **Marjory Pompilus:** investigation, formal analysis. **Rawad Daniel Arja:** investigation, formal analysis. **Tian Zhu:** investigation. **Zhihui Yang:** conceptualization, investigation, data curation, project administration, formal analysis. **Yueqiang Fu:** investigation. **Jiepei Zhu:** conceptualization, investigation, writing (review editing), supervision, project administration. **Firas Kobeissy:** conceptualization, writing (review and editing), supervision, project administration. **Kevin K.W. Wang:** conceptualization (lead), methodology, validation, resources, writing (review editing), supervision, project administration, funding acquisition (lead). **Marcelo Febo:** conceptualization, resources, writing (review and editing), software (lead), formal analysis (lead), investigation, data curation, visualization, supervision, project administration, funding acquisition.

Author Disclosure Statement

No conflicts to disclose.

Transparency, Rigor and Reproducibility Summary

Study registration. This is a preclinical study registered at the National Institute on Neurological Disorders and Stroke (NINDS) as one of the Translational Outcomes in NeuroTrauma (TOP-NT) UG3 phase studies (grant UG3NS106938). The study is now complete, and the data is made available through the odc-tbi.org preclinical TBI repository. **Analytical plan specification.** This is an animal study. As such its analysis plan was not formally pre-registered, but the team members with primary responsibility for the analysis (e.g., lead and co-authors) certify that the data analysis plan was pre-specified. **Statistical power and sample size calculations.** Power analyses conducted during the planning stages for the original proposal prior to funding of the research. With the aid of data from preliminary experiments and in some instances using data from studies with similar outcome measures, number of independent variables, and assuming effect sizes within a similar range we determined the number of animals with the objective of achieving a power of at least 0.8. For instance, using G*Power version 3.1.9.2 (University of Dusseldorf), it was determined that the selection of n of at least 16 per condition provided a power of 0.97. **Actual sample size.** Sample sizes varied slightly from those planned with sample size calculations. However, the final sample sizes carried sufficient power and is within range of prior data measuring similar

imaging outcomes. **Blinding with assessment of adequacy.** Image processing involved the renaming of individual data sets that allowed blinding. In this preclinical study, rats were provided by the collaborative laboratory to the imaging laboratory using identifiers that were revealed at the end of the data acquisition. **Source and reproducibility of imaging acquisition and analytical approaches**[7] All imaging equipment and analytical software are either commercial (e.g., Bruker) or freely available under GNU license. **Validity of clinically relevant assessments.** This is a preclinical animal study. **Assumptions of statistical tests assessed.** We assumed a 2 x 2 analysis of variance, with medium effect sizes of 0.6, 4 groups, error probability of 0.05, gives critical F of 2.8. **Multiple comparisons management.** Benjamini-Hochberg false discovery rate correction was used for multiple comparisons management. **Replication/external validation.** Ongoing studies as part of the UH3 phase of this TOP-NT grant are assessing reproducibility methods harmonization across several laboratories. **Data availability.** Data will be made available via odc-tbi.org. **Code availability.** No new code was generated as part of this study.

References

1. Demlie TA, Alemu MT, Messelu MA, et al. Incidence and predictors of mortality among traumatic brain injury patients admitted to Amhara region Comprehensive Specialized Hospitals, northwest Ethiopia, 2022. BMC Emerg Med 2023;23(1):55, doi:10.1186/s12873-023-00823-9
2. Bramlett HM, Dietrich WD. Long-Term Consequences of Traumatic Brain Injury: Current Status of Potential Mechanisms of Injury and Neurological Outcomes. J Neurotrauma 2015;32(23):1834-48, doi:10.1089/neu.2014.3352
3. Vella MA, Crandall ML, Patel MB. Acute Management of Traumatic Brain Injury. Surg Clin North Am 2017;97(5):1015-1030, doi:10.1016/j.suc.2017.06.003
4. Wang KK, Yang Z, Zhu T, et al. An update on diagnostic and prognostic biomarkers for traumatic brain injury. Expert Rev Mol Diagn 2018;18(2):165-180, doi:10.1080/14737159.2018.1428089
5. Sharp DJ, Beckmann CF, Greenwood R, et al. Default mode network functional and structural connectivity after traumatic brain injury. Brain 2011;134(Pt 8):2233-47, doi:10.1093/brain/awr175
6. Alhourani A, Wozny TA, Krishnaswamy D, et al. Magnetoencephalography-based identification of functional connectivity network disruption following mild traumatic brain injury. J Neurophysiol 2016;116(4):1840-1847, doi:10.1152/jn.00513.2016
7. Bernier RA, Roy A, Venkatesan UM, et al. Dedifferentiation Does Not Account for Hyperconnectivity after Traumatic Brain Injury. Front Neurol 2017;8(297, doi:10.3389/fneur.2017.00297
8. Grossner EC, Bernier RA, Brenner EK, et al. Enhanced default mode connectivity predicts metacognitive accuracy in traumatic brain injury. Neuropsychology 2019;33(7):922-933, doi:10.1037/neu0000559

9. Hillary FG, Slocomb J, Hills EC, et al. Changes in resting connectivity during recovery from severe traumatic brain injury. Int J Psychophysiol 2011;82(1):115-23, doi:10.1016/j.ijpsycho.2011.03.011

10. Virji-Babul N, Hilderman CG, Makan N, et al. Changes in functional brain networks following sports-related concussion in adolescents. J Neurotrauma 2014;31(23):1914-9, doi:10.1089/neu.2014.3450

11. Cao C, Slobounov S. Alteration of cortical functional connectivity as a result of traumatic brain injury revealed by graph theory, ICA, and sLORETA analyses of EEG signals. IEEE Trans Neural Syst Rehabil Eng 2010;18(1):11-9, doi:10.1109/TNSRE.2009.2027704

12. Sakthivel R, Criado-Marrero M, Barroso D, et al. Fixed Time-Point Analysis Reveals Repetitive Mild Traumatic Brain Injury Effects on Resting State Functional Magnetic Resonance Imaging Connectivity and Neuro-Spatial Protein Profiles. J Neurotrauma 2023;40(19-20):2037-2049, doi:10.1089/neu.2022.0464

13. Kulkarni P, Morrison TR, Cai X, et al. Neuroradiological Changes Following Single or Repetitive Mild TBI. Front Syst Neurosci 2019;13(34, doi:10.3389/fnsys.2019.00034

14. Harris NG, Verley DR, Gutman BA, et al. Disconnection and hyper-connectivity underlie reorganization after TBI: A rodent functional connectomic analysis. Exp Neurol 2016;277(124-138, doi:10.1016/j.expneurol.2015.12.020

15. Yang Z, Zhu T, Pompilus M, et al. Compensatory functional connectome changes in a rat model of traumatic brain injury. Brain Commun 2021;3(4):fcab244, doi:10.1093/braincomms/fcab244

16. Mohamed AZ, Cumming P, Nasrallah FA. Traumatic brain injury augurs ill for prolonged deficits in the brain's structural and functional integrity following controlled cortical impact injury. Sci Rep 2021;11(1):21559, doi:10.1038/s41598-021-00660-5

17. Yang L, Benardo LS, Valsamis H, et al. Acute injury to superficial cortex leads to a decrease in synaptic inhibition and increase in excitation in neocortical layer V pyramidal cells. J Neurophysiol 2007;97(1):178-87, doi:10.1152/jn.01374.2005

18. Harris NG, Verley DR, Gutman BA, et al. Bi-directional changes in fractional anisotropy after experiment TBI: Disorganization and reorganization? Neuroimage 2016;133(129-143, doi:10.1016/j.neuroimage.2016.03.012

19. Zheng T, Du J, Yuan Y, et al. Effect of Low Intensity Transcranial Ultrasound (LITUS) on Post-traumatic Brain Edema in Rats: Evaluation by Isotropic 3-Dimensional T2 and Multi-TE T2 Weighted MRI. Front Neurol 2020;11(578638, doi:10.3389/fneur.2020.578638

20. Alder J, Fujioka W, Lifshitz J, et al. Lateral fluid percussion: model of traumatic brain injury in mice. J Vis Exp 2011;54), doi:10.3791/3063

21. Lifshitz J, Rowe RK, Griffiths DR, et al. Clinical relevance of midline fluid percussion brain injury: Acute deficits, chronic morbidities and the utility of biomarkers. Brain Inj 2016;30(11):1293-1301, doi:10.1080/02699052.2016.1193628

22. Radabaugh H, Bonnell J, Schwartz O, et al. Use of Machine Learning to Re-Assess Patterns of Multivariate Functional Recovery after Fluid Percussion Injury: Operation Brain Trauma Therapy. J Neurotrauma 2021;38(12):1670-1678, doi:10.1089/neu.2020.7357

23. Kochanek PM, Bramlett HM, Dixon CE, et al. Operation Brain Trauma Therapy: 2016 Update. Mil Med 2018;183(suppl_1):303-312, doi:10.1093/milmed/usx184

24. Cox RW. AFNI: software for analysis and visualization of functional magnetic resonance neuroimages. Comput Biomed Res 1996;29(3):162-73, doi:10.1006/cbmr.1996.0014

25. Jenkinson M, Bannister P, Brady M, et al. Improved optimization for the robust and accurate linear registration and motion correction of brain images. Neuroimage 2002;17(2):825-41, doi:10.1016/s1053-8119(02)91132-8

26. Klein A, Andersson J, Ardekani BA, et al. Evaluation of 14 nonlinear deformation algorithms applied to human brain MRI registration. Neuroimage 2009;46(3):786-802, doi:10.1016/j.neuroimage.2008.12.037

27. Yushkevich PA, Piven J, Hazlett HC, et al. User-guided 3D active contour segmentation of anatomical structures: significantly improved efficiency and reliability. Neuroimage 2006;31(3):1116-28, doi:10.1016/j.neuroimage.2006.01.015

28. Xia M, Wang J, He Y. BrainNet Viewer: a network visualization tool for human brain connectomics. PLoS One 2013;8(7):e68910, doi:10.1371/journal.pone.0068910

29. Rubinov M, Sporns O. Complex network measures of brain connectivity: uses and interpretations. Neuroimage 2010;52(3):1059-69, doi:10.1016/j.neuroimage.2009.10.003

30. Smith SM, Jenkinson M, Woolrich MW, et al. Advances in functional and structural MR image analysis and implementation as FSL. Neuroimage 2004;23 Suppl 1(S208-19, doi:10.1016/j.neuroimage.2004.07.051

31. Schmidt KF, Ziu M, Schmidt NO, et al. Volume reconstruction techniques improve the correlation between histological and in vivo tumor volume measurements in mouse models of human gliomas. J Neurooncol 2004;68(3):207-15, doi:10.1023/b:neon.0000033364.43142.bf

32. Schneider CA, Rasband WS, Eliceiri KW. NIH Image to ImageJ: 25 years of image analysis. Nat Methods 2012;9(7):671-5, doi:10.1038/nmeth.2089

33. Recanzone GH, Merzenich MM, Jenkins WM, et al. Topographic reorganization of the hand representation in cortical area 3b owl monkeys trained in a frequency-discrimination task. J Neurophysiol 1992;67(5):1031-56, doi:10.1152/jn.1992.67.5.1031

34. Xerri C, Coq JO, Merzenich MM, et al. Experience-induced plasticity of cutaneous maps in the primary somatosensory cortex of adult monkeys and rats. J Physiol Paris 1996;90(3-4):277-87, doi:10.1016/s0928-4257(97)81438-6

35. Xerri C, Merzenich MM, Peterson BE, et al. Plasticity of primary somatosensory cortex paralleling sensorimotor skill recovery from stroke in adult monkeys. J Neurophysiol 1998;79(4):2119-48, doi:10.1152/jn.1998.79.4.2119

36. Yang L, Afroz S, Michelson HB, et al. Spontaneous epileptiform activity in rat neocortex after controlled cortical impact injury. J Neurotrauma 2010;27(8):1541-8, doi:10.1089/neu.2009.1244

37. Mishra AM, Bai X, Sanganahalli BG, et al. Decreased resting functional connectivity after traumatic brain injury in the rat. PLoS One 2014;9(4):e95280, doi:10.1371/journal.pone.0095280

38. Verley DR, Torolira D, Pulido B, et al. Remote Changes in Cortical Excitability after Experimental Traumatic Brain Injury and Functional Reorganization. J Neurotrauma 2018;35(20):2448-2461, doi:10.1089/neu.2017.5536

39. Sanganahalli BG, Herman P, Hyder F, et al. Mitochondrial functional state impacts spontaneous neocortical activity and resting state FMRI. PLoS One 2013;8(5):e63317, doi:10.1371/journal.pone.0063317

40. Andrews BT, Barbay S, Townsend J, et al. Unrepaired decompressive craniectomy worsens motor performance in a rat traumatic brain injury model. Sci Rep 2020;10(1):22242, doi:10.1038/s41598-020-79155-8

41. Wu J, He J, Tian X, et al. Activation of the Hedgehog Pathway Promotes Recovery of Neurological Function After Traumatic Brain Injury by Protecting the Neurovascular Unit. Transl Stroke Res 2020;11(4):720-733, doi:10.1007/s12975-019-00771-2

42. Schneider G, Fries P, Wagner-Jochem D, et al. Pathophysiological changes after traumatic brain injury: comparison of two experimental animal models by means of MRI. MAGMA 2002;14(3):233-41, doi:10.1007/BF02668217

43. Kochanek PM, Hendrich KS, Dixon CE, et al. Cerebral blood flow at one year after controlled cortical impact in rats: assessment by magnetic resonance imaging. J Neurotrauma 2002;19(9):1029-37, doi:10.1089/089771502760341947

44. Forbes ML, Hendrich KS, Kochanek PM, et al. Assessment of cerebral blood flow and CO2 reactivity after controlled cortical impact by perfusion magnetic resonance imaging using arterial spin-labeling in rats. J Cereb Blood Flow Metab 1997;17(8):865-74, doi:10.1097/00004647-199708000-00005

45. Long JA, Watts LT, Li W, et al. The effects of perturbed cerebral blood flow and cerebrovascular reactivity on structural MRI and behavioral readouts in mild traumatic brain injury. J Cereb Blood Flow Metab 2015;35(11):1852-61, doi:10.1038/jcbfm.2015.143

46. Zhang F, Sprague SM, Farrokhi F, et al. Reversal of attenuation of cerebrovascular reactivity to hypercapnia by a nitric oxide donor after controlled cortical impact in a rat model of traumatic brain injury. J Neurosurg 2002;97(4):963-9, doi:10.3171/jns.2002.97.4.0963

47. Hendrich KS, Kochanek PM, Williams DS, et al. Early perfusion after controlled cortical impact in rats: quantification by arterial spin-labeled MRI and the influence of spin-lattice relaxation time heterogeneity. Magn Reson Med 1999;42(4):673-81, doi:10.1002/(sici)1522-2594(199910)42:4<673::aid-mrm8>3.0.co;2-b

48. Yu M, Wang M, Yang D, et al. Dynamics of blood brain barrier permeability and tissue microstructure following controlled cortical impact injury in rat: A dynamic contrast-enhanced magnetic resonance imaging and diffusion kurtosis imaging study. Magn Reson Imaging 2019;62(1-9, doi:10.1016/j.mri.2019.01.017

49. Missault S, Anckaerts C, Blockx I, et al. Neuroimaging of Subacute Brain Inflammation and Microstructural Changes Predicts Long-Term Functional Outcome after Experimental Traumatic Brain Injury. J Neurotrauma 2019;36(5):768-788, doi:10.1089/neu.2018.5704

50. Li W, Long JA, Watts L, et al. Spatiotemporal changes in diffusion, T2 and susceptibility of white matter following mild traumatic brain injury. NMR Biomed 2016;29(7):896-903, doi:10.1002/nbm.3536

51. Manninen E, Chary K, Lapinlampi N, et al. Acute thalamic damage as a prognostic biomarker for post-traumatic epileptogenesis. Epilepsia 2021;62(8):1852-1864, doi:10.1111/epi.16986

52. Bhagavatula S, Cabeen R, Harris NG, et al. Image data harmonization tools for the analysis of post-traumatic epilepsy development in preclinical multisite MRI studies. Epilepsy Res 2023;195(107201, doi:10.1016/j.eplepsyres.2023.107201

53. Nielson JL, Paquette J, Liu AW, et al. Topological data analysis for discovery in preclinical spinal cord injury and traumatic brain injury. Nat Commun 2015;6(8581, doi:10.1038/ncomms9581

Figure Legends

Figure 1 Regions of interest (ROIs) were manually created over a multi-subject template to extract fMRI signals for connectivity analysis. A) Coronal view of the distribution of bilateral cortical, hippocampal and striatal ROIs. B) 3D renditions of the ROIs to illustrate the volumetric sampling across brain regions. C) Nomenclature used to identify ROIs individually across the cortical mantle, medially and laterally in each hemisphere, and in subcortical regions. Abbreviations: C-MC, contralateral-medial cortex; Ip-MC, ipsilateral-medial cortex; C-LC, contralateral-lateral cortex; Ip-LC, ipsilateral-lateral cortex; C-Str, contralateral striatum; Ip-Str, ipsilateral striatum; C-Hpc, contralateral hippocampus; Ip-Hpc, ipsilateral hippocampus.

Figure 2 Controlled cortical impact (CCI) and Lateral fluid percussion injury (LFPI) both increased node strength in contralateral cortex and reduced it in ipsilateral cortex. A) group averaged 3D functional connectome maps of control rats illustrating basal node strength values. B) Connectome map showing increases contralateral node strength and intra-hemispheric cortical connectivity in CCI rats at day 2. C) Connectome map showing increases contralateral node strength and intra-hemispheric cortical connectivity in LFPI rats at day 2. D) Connectome map showing increased contralateral node strength and intra-hemispheric cortical connectivity still present in CCI rats at day 30. E) Connectome map showing similar node strength and intra-hemispheric connectivity in both cortical hemispheres in LFPI rats at day 30. In A-E, node size is representative of the calculated ROI node strength and edges (connecting lines) are Fisher's z-transformed Pearson correlation coefficient (maps threshold is 12% edge density; scale bar adjoining each map indicates z range). F) Heat maps of node strength across the sampled ROIs in all groups. Left y axis shows ROI name and x axis group. Asterisks on the right indicate significant difference between specific groups (linear mixed effects ANOVA with repeated measures; false discovery rate corrected $q<0.05$). The scale bar to the left indicates averaged node strength value. *CCI day 2 vs control; ** LFPI day 2 vs control; ***CCI day 30 vs LFPI day 30; ****LFPI day 2 vs day 30; *****CCI day 30 vs controls; ******CCI day 2 vs LFPI day 2. Controls, n= 26; CCI day 2, n = 30; CCI day 30, n = 12; LFPI day 2, n = 13; LFPI day 30, n = 8.

Figure 3 Cortical brain areas affected by CCI vs LFPI. The brain regions were identified by overlaying group averaged ROI's showing significant differences between either CCI or LFPI and controls onto a rat brain template and parcellation[13]. A) Regions with increases and decreases in node strength on day 2 following CCI include sensorimotor areas in both left and

right hemispheres. B) By day 30 after CCI, parietal and visual areas shown decreases in ipsilateral cortex. C) Regions affected by LFPI include many of the same cortical areas as CCI on day 2. D) Functional connectivity differences are no longer measured on day 30 following LFPI.

Figure 4 Representative diffusion tensor and T2 maps of a control, CCI and LFPI rats. Shown are a B0 image, fractional anisotropy (FA) grey scale map and mean, axial and radial diffusivity maps (MD, AD, and RD, respectively), and a representative T2 maps of a control animal. Right side is the injury side. The approximate craniotomy/impact site (red bars) for CCI and the craniotomy site for LFPI (blue bars) are shown.

Figure 5 White matter (WM) and cortical tissue diffusion changes at 2 and 30 days following CCI or LFPI. A-D) FA, MD, AD, and RD in ipsi and contralateral WM and cortex. Data are shown as box and Tukey whisker plots (symbols denote outliers). Lines and asterisks indicate significant differences at $p<0.05$ (Two-way ANOVA followed by Tukey's multiple comparison post hoc test; *$p<0.05$, **$p<0.005$, ***$p<0.0005$; ****$p<0.00005$). Black color filled boxes is control, grey is CCI, and hatched bar is LFPI. Controls, n= 25; CCI day 2, n = 28; CCI day 30, n = 9; LFPI day 2, n = 13; LFPI day 30, n = 7.

Figure 6 T2 (in ms) in ipsi and contralateral WM and cortex of control, CCI and LFPI exposed rats on days 2 and 30 post-TBI. Data are shown as box and Tukey whisker plots (symbols denote outliers). Lines and asterisks indicate significant differences at $p<0.05$ (Two-way ANOVA followed by Tukey's multiple comparison post hoc test; *$p<0.05$, **$p<0.005$). Black color filled boxes is control, grey is CCI, and hatched bar is LFPI. Controls, n= 16; CCI day 2, n = 16; CCI day 30, n = 9; LFPI day 2, n = 12; LFPI day 30, n = 7.

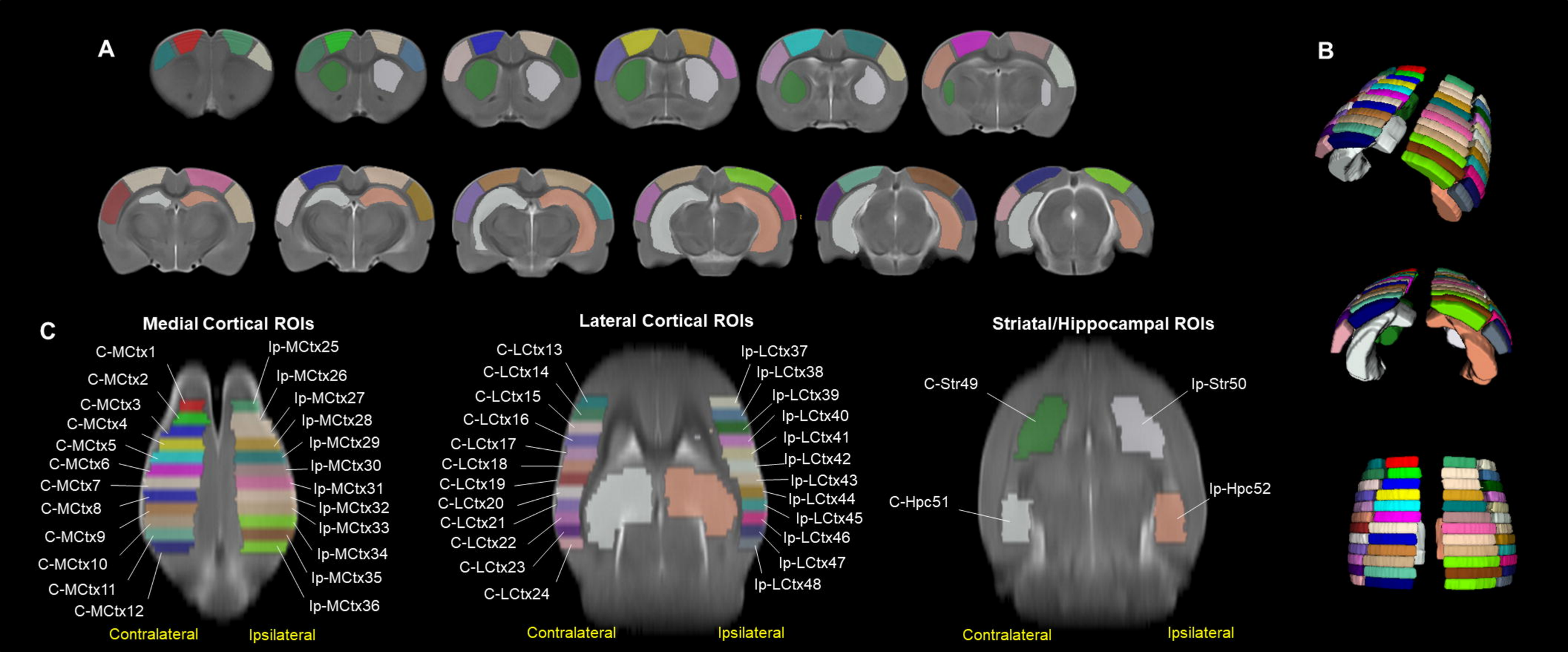
A
B
C
Medial Cortical ROIs
C-MCtx1
C-MCtx2
C-MCtx3
C-MCtx4
C-MCtx5
C-MCtx6
C-MCtx7
C-MCtx8
C-MCtx9
C-MCtx10
C-MCtx11
C-MCtx12
Ip-MCtx25
Ip-MCtx26
Ip-MCtx27
Ip-MCtx28
Ip-MCtx29
Ip-MCtx30
Ip-MCtx31
Ip-MCtx32
Ip-MCtx33
Ip-MCtx34
Ip-MCtx35
Ip-MCtx36
Contralateral
Ipsilateral
Lateral Cortical ROIs
C-LCtx13
C-LCtx14
C-LCtx15
C-LCtx16
C-LCtx17
C-LCtx18
C-LCtx19
C-LCtx20
C-LCtx21
C-LCtx22
C-LCtx23
C-LCtx24
Ip-LCtx37
Ip-LCtx38
Ip-LCtx39
Ip-LCtx40
Ip-LCtx41
Ip-LCtx42
Ip-LCtx43
Ip-LCtx44
Ip-LCtx45
Ip-LCtx46
Ip-LCtx47
Ip-LCtx48
Contralateral
Ipsilateral
Striatal/Hippocampal ROIs
C-Str49
Ip-Str50
C-Hpc51
Ip-Hpc52
Contralateral
Ipsilateral

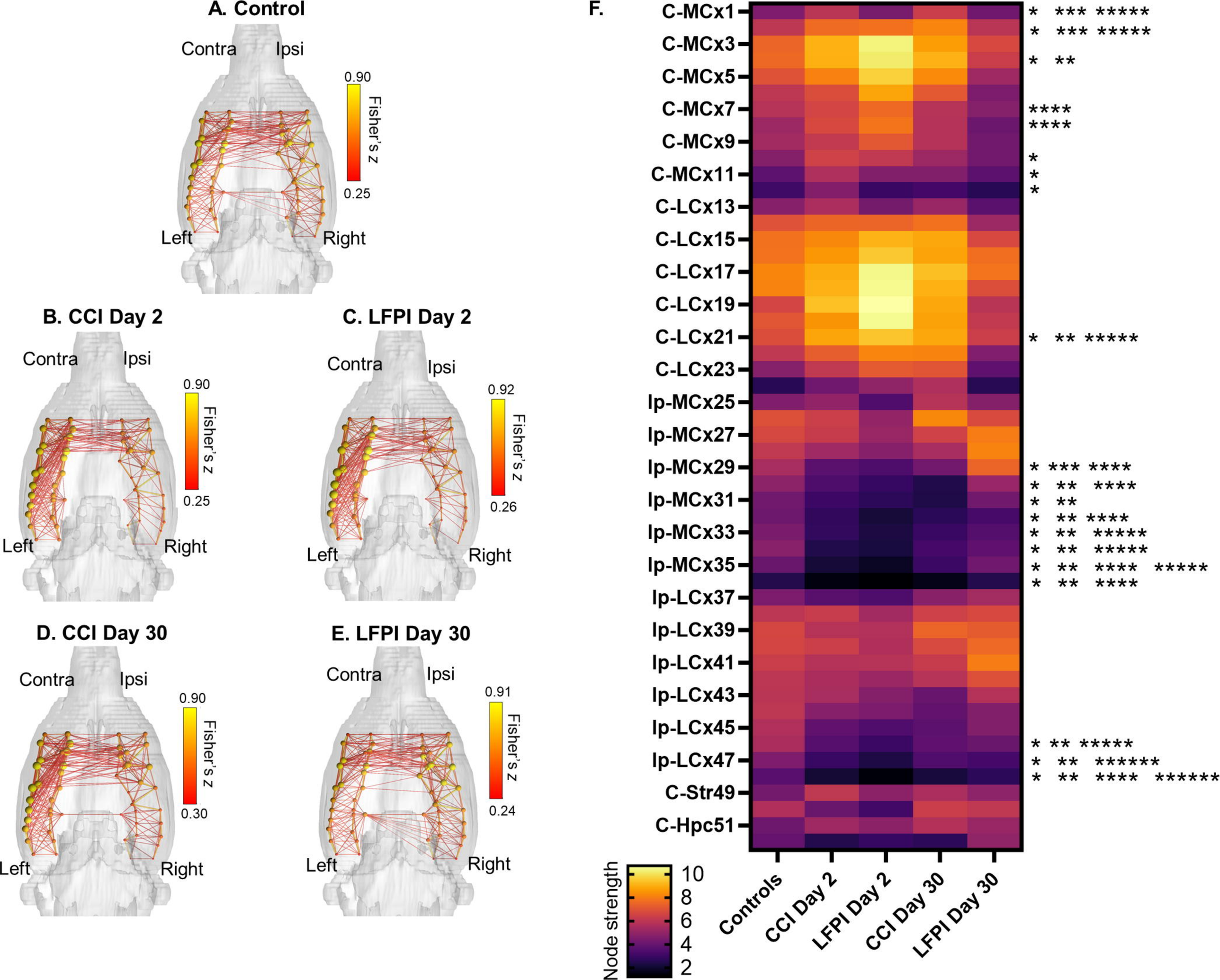
A. Control
Contra
Ipsi
0.90
Fisher's z
0.25
Left
Right
B. CCI Day 2
Contra
Ipsi
0.90
Fisher's z
0.25
Left
Right
C. LFPI Day 2
Contra
Ipsi
0.92
Fisher's z
0.26
Left
Right
D. CCI Day 30
Contra
Ipsi
0.90
Fisher's z
0.30
Left
Right
E. LFPI Day 30
Contra
Ipsi
0.91
Fisher's z
0.24
Left
Right
F.
C-MCx1
C-MCx3
C-MCx5
C-MCx7
C-MCx9
C-MCx11
C-LCx13
C-LCx15
C-LCx17
C-LCx19
C-LCx21
C-LCx23
Ip-MCx25
Ip-MCx27
Ip-MCx29
Ip-MCx31
Ip-MCx33
Ip-MCx35
Ip-LCx37
Ip-LCx39
Ip-LCx41
Ip-LCx43
Ip-LCx45
Ip-LCx47
C-Str49
C-Hpc51
Controls
CCI Day 2
LFPI Day 2
CCI Day 30
LFPI Day 30
Node strength
10
8
6
4
2

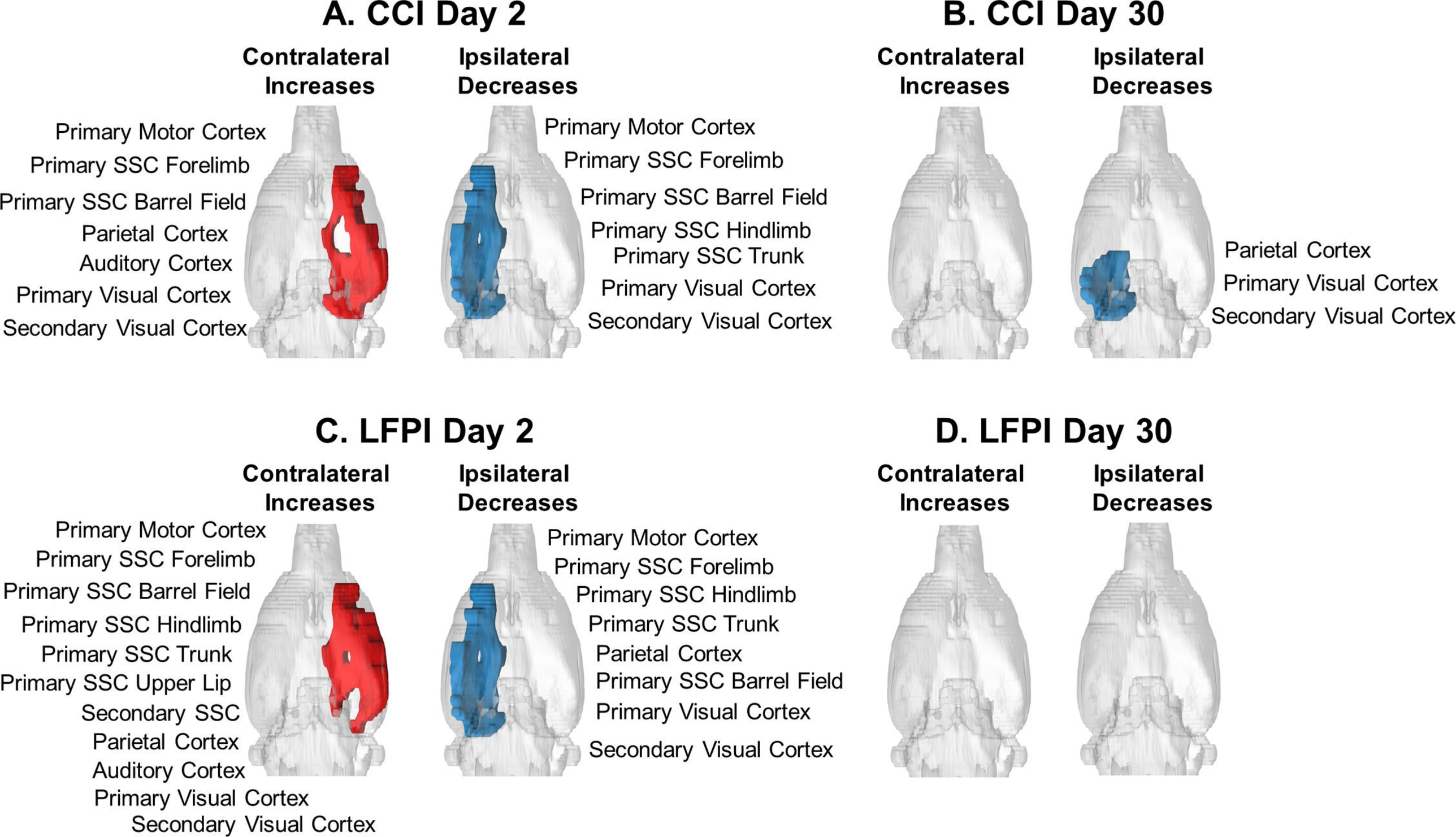
A. CCI Day 2
Contralateral Increases
Ipsilateral Decreases
Primary Motor Cortex
Primary SSC Forelimb
Primary SSC Barrel Field
Parietal Cortex
Auditory Cortex
Primary Visual Cortex
Secondary Visual Cortex
Primary Motor Cortex
Primary SSC Forelimb
Primary SSC Barrel Field
Primary SSC Hindlimb
Primary SSC Trunk
Primary Visual Cortex
Secondary Visual Cortex
B. CCI Day 30
Contralateral Increases
Ipsilateral Decreases
Parietal Cortex
Primary Visual Cortex
Secondary Visual Cortex
C. LFPI Day 2
Contralateral Increases
Ipsilateral Decreases
Primary Motor Cortex
Primary SSC Forelimb
Primary SSC Barrel Field
Primary SSC Hindlimb
Primary SSC Trunk
Primary SSC Upper Lip
Secondary SSC
Parietal Cortex
Auditory Cortex
Primary Visual Cortex
Secondary Visual Cortex
Primary Motor Cortex
Primary SSC Forelimb
Primary SSC Hindlimb
Primary SSC Trunk
Parietal Cortex
Primary SSC Barrel Field
Primary Visual Cortex
Secondary Visual Cortex
D. LFPI Day 30
Contralateral Increases
Ipsilateral Decreases

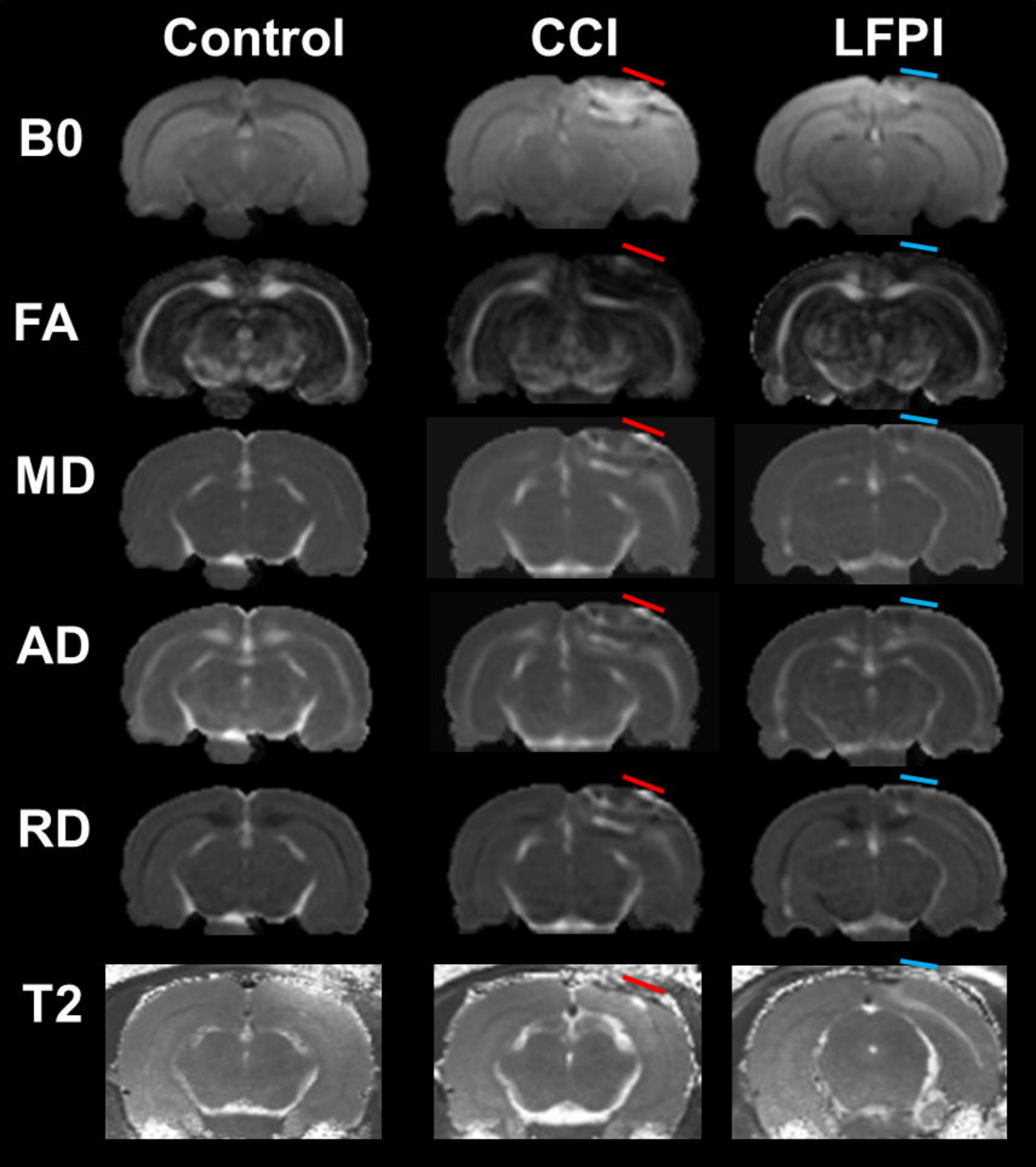
Control
CCI
LFPI
B0
FA
MD
AD
RD
T2

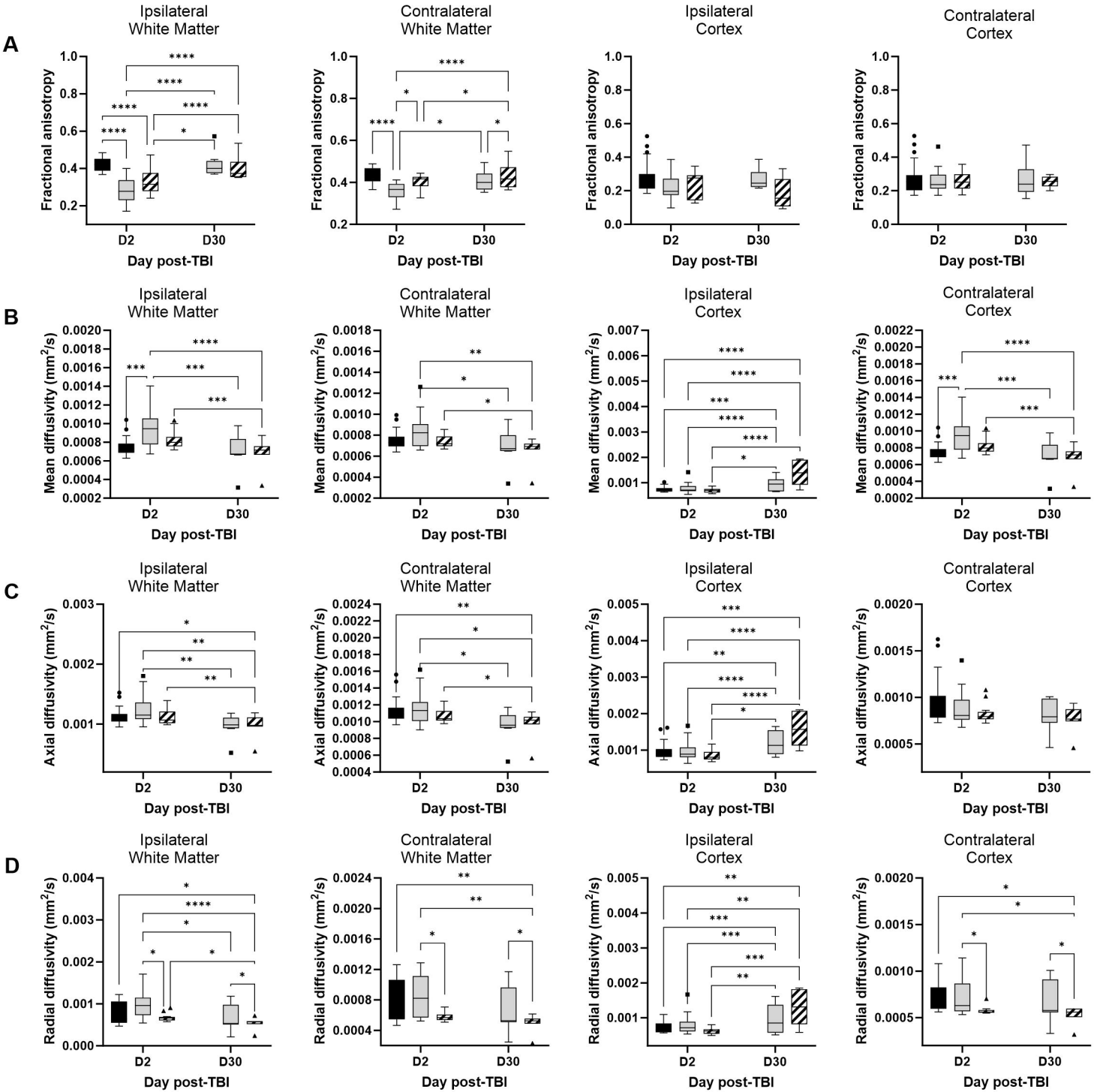
A
Ipsilateral White Matter
Contralateral White Matter
Ipsilateral Cortex
Contralateral Cortex
Fractional anisotropy
Day post-TBI
D2
D30
B
Mean diffusivity (mm²/s)
C
Axial diffusivity (mm²/s)
D
Radial diffusivity (mm²/s)

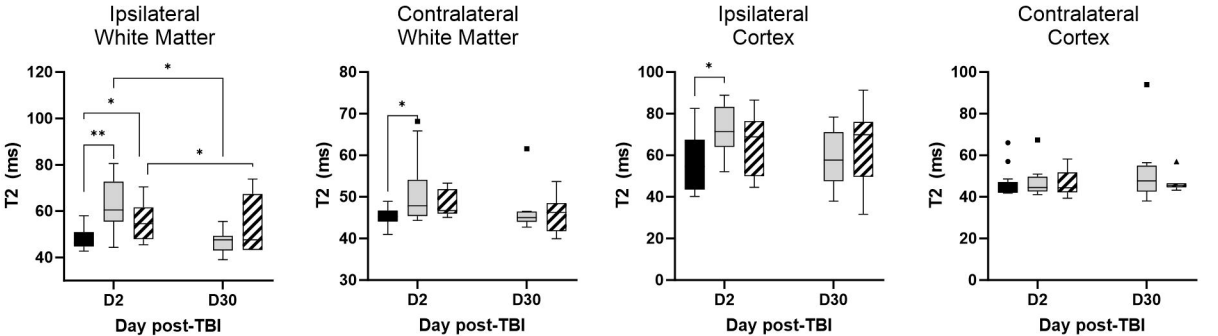
Ipsilateral
White Matter
Contralateral
White Matter
Ipsilateral
Cortex
Contralateral
Cortex
T2 (ms)
Day post-TBI
D2
D30
*
**